Sensors and Materials, Vol. 31, No. 7 (2019) 2271–2279
MYU Tokyo

S & M 1930

Vertical Hot-electron Terahertz Detectors Based on Black-$As_{1-x}P_x$/graphene/black-$As_{1-y}P_y$ Heterostructures

Maxim Ryzhii,[1] Victor Ryzhii,[2,3,4,5*] Vladimir Mitin,[2,6]
Michael Shur,[7] and Taiichi Otsuji[2]

[1]Department of Computer Science and Engineering, University of Aizu, Aizu-Wakamatsu 965-8580, Japan
[2]Research Institute of Electrical Communication, Tohoku University, Sendai 980-8577, Japan
[3]Mokerov Institute of Ultra High Frequency Semiconductor Electronics of RAS, Moscow 105005, Russia
[4]Center of Photonics and Infrared Technology, Bauman Moscow State Technical University, Moscow 11105, Russia
[5]Center of Photonics and Two-Dimensional Materials, Moscow Institute of Physics and Technology, Dolgoprudny 141700, Russia
[6]Department of Electrical Engineering, University at Buffalo, SUNY, Buffalo, NY 1460-1920, USA
[7]Department of Electrical, Computer, and Systems Engineering, Rensselaer Polytechnic Institute, Troy, NY 12180, USA

(Received January 21, 2019; accepted April 5, 2019)

Keywords: hot electron, terahertz, photodetector, graphene, black arsenic, black phosphorus, heterostructure

We propose and evaluate vertical hot-electron terahertz (THz) detectors based on black-$As_{1-x}P_x$/graphene/black-$As_{1-y}P_y$ (b-AsP/G/b-AsP) heterostructures. The operation of these detectors is associated with the thermionic emission of the electrons heated in the graphene layer (G-layer) by incoming THz radiation stimulating the electron injection from the emitter, i.e., with the hot-electron bolometric mechanism. The combination of the effective electron heating in the G-layer with the features of the b-$As_{1-x}P_x$ and b-$As_{1-y}P_y$ band structures with a proper relation between the b-P fractions, x and y ($x \geq y$), might result in the high photoconductive gain and detector responsivity of the proposed detectors. As discussed, these detectors can surpass the similar bolometric detectors based on graphene-based heterostructures with relatively high energy barriers for the electrons and holes in the G-layers and the bolometric detectors based on III-V quantum wells.

1. Introduction

Owing to the gapless energy spectrum,[1] the heterostructures based on the graphene layers (G-layers) can be used in different optoelectronic devices using the interband transitions in the terahertz (THz) and far-infrared (FIR) spectral ranges. High electron and hole mobilities in the G-layers accompanied by a high energy of optical phonons ($\hbar\omega_0 \simeq 200$ meV) provide a relatively long carrier energy relaxation time of "warm" electrons.[2] This enables the use of the G-layers and more complex G-structures in bolometric detectors of THz and FIR radiations,[2,3] particularly in the bolometric THz detector based on vertical structures in which

*Corresponding author: e-mail: v-ryzhii@riec.tohoku.ac.jp
https://doi.org/10.18494/SAM.2019.2305

ISSN 0914-4935

the G-layer serving as a sensitive element is sandwiched between wide-gap barrier layers.[4] Such photodetectors exploit the thermionic emission of the electrons heated in the G-layer by THz radiation. The characteristics of the barrier-G-layer-barrier detectors in question depend on the band alignment of the barrier materials and G-layer, particularly in terms of conduction band offsets.[5,6] In this regard, the heterostructures with the G-layer sandwiched between the barriers composed of black-arsenic-phosphorus (b-$As_{1-x}P_x$ and b-$As_{1-y}P_y$) layers[7,8] with the optimized x and y values can work well for THz detectors. The bulk compounds b-$As_{1-x}P_x$ have an energy gap varying from Δ_G ~300 meV for $x = 1$ to Δ_G ~150 meV for $x \simeq 0$. The band alignment of these materials with the G-layer corresponds to the Dirac point falling between their valence band top and the conduction band bottom. As a result, the heights of the barriers, Δ_E and Δ_C, for the electrons in the G-layers sandwiched between b-$As_{1-x}P_x$ and b-$As_{1-y}P_y$ are relatively small. The latter reinforces the thermionic electron emission from the G-layers into such barrier layers. The b-$As_{1-x}P_x$ compounds were already used in different heterostructure devices.[9–13] The pertinent technology is developed rapidly, and its prospects appear to be very promising.

In this paper, we propose and evaluate THz detectors using b-$As_{1-x}P_x$/G/b-$As_{1-y}P_y$ heterostructures, i.e., N-n-N-heterostructures with specific materials for N-barrier layers. In these detectors, the radiation-sensitive n-doped layer enables the intraband (Drude) absorption of the THz radiation. We demonstrate that these THz detectors can exhibit a fairly high responsivity in a wide range of THz frequencies. The enhanced detector performance is associated with the high efficiency of electron heating in the G-layer, relatively low energy barriers between the b-$As_{1-x}P_x$ and b-$As_{1-y}P_y$ layers and the G-layer, and the possibility of a strong photoconductive gain because of a low capture probability of the electrons injected via the b-$As_{1-x}P_x$ emitter layer into the G-layer (particularly, when $x > y$).

2. Detector Structure and Operation Principle

Figure 1 shows the band diagram of a THz detector under consideration at the operation bias voltage. The emitter and collector barrier layers are the undoped or lightly doped b-$As_{1-x}P_x$ and b-$As_{1-y}P_y$ layers, respectively. The n-doped G-layer serves as the detector base sensitive to the incident THz radiation. For the highly doped emitter and collector contact regions, the same materials as those for the barrier layer (as shown in Fig. 1) or other more wide-gap materials are used. In the heterostructures with the latter contact regions, the injection from the emitter contact can involve tunneling. The operation of these detectors is associated with the thermionic emission of the electrons heated by the incoming THz radiation absorbed in this layer due to the Drude absorption mechanism. The emitted warm electrons propagate across the b-$As_{1-y}P_y$ barrier with $y \leq x$, contribute to the net terminal current, and are collected by the N^+ collector. The electron emission from the G-layer caused by the THz radiation leads to the net charge in the G-layer (the donor charge becomes uncompensated). This charge increases the electric field in the emitter barrier layer and, hence, leads to the injection of extra electrons from the N^+ emitter. The flux of these electrons can markedly exceed that of the electrons emitted from the G-layer provided that the fraction of electrons captured into the G-layer is small. Since the

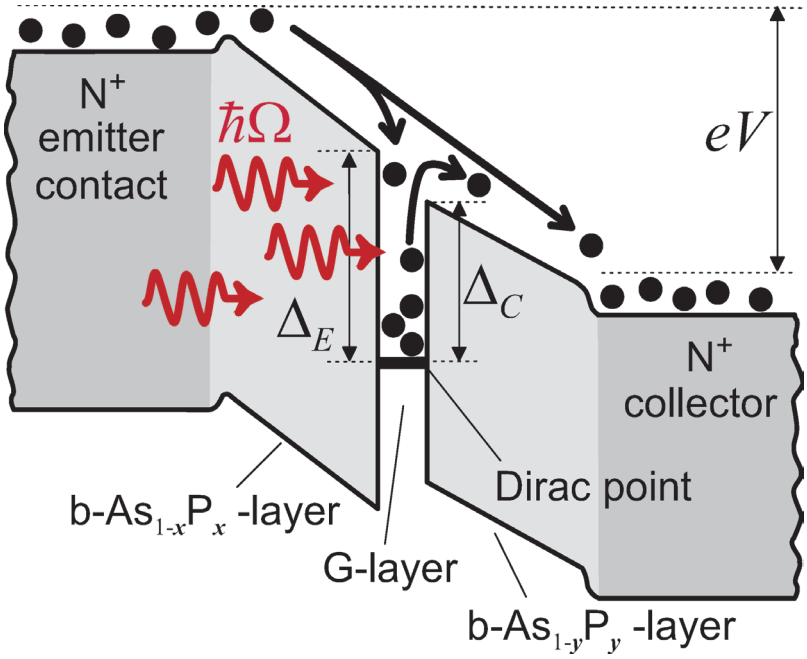

Fig. 1. (Color online) Schematic band diagram of a THz detector based on a b-$As_{1-x}P_x$/G/b-$As_{1-y}P_y$ heterostructure ($x > y$) at sufficiently high bias voltage V. Circles and smooth arrows correspond to the electrons injected from the N^+ emitter contact, propagating across the barrier layers, captured into and emitted from the G-layer (both in the dark and under THz irradiation).

injected electrons propagating across the emitter layer can acquire a significant kinetic energy, their capture probability into the G-layer can be very small.[14–16]

3. Model and Characteristics

Considering that, under the stationary condition, the electron flux from the G-layer is equal to the flux of the electrons coming from the emitter and captured into the G-layer, the net terminal current density at sufficiently high bias voltages ($V >> k_BT_0/e$) following Ref. 4 can be presented as

$$j = \frac{e\Sigma}{\tau_{esc} p_c} \exp\left(\frac{\mu - \Delta_C}{k_B T}\right), \tag{1}$$

where Σ is the electron density in the G-layer, μ is the electron Fermi energy in the G-layer determined by its doping level, e is the electron charge, k_B, T_0, and T are the Boltzmann constant, lattice temperature, and effective electron temperature in the G-layer, respectively, τ_{esc} is the characteristic escape time of the electrons with the energy $\varepsilon > \Delta_C$ from the G-layer (τ_{esc} has the same order of magnitude as the electron momentum relaxation time in the G-layers, τ), Δ_C is the conduction band offset in the G-layer and collector b-$As_{1-y}P_y$-layer, and p_c is the

capture probability.[14–16] The concept of the capture parameter[14] assumes that the emitter contact is able to produce a sufficient injected electron current density required to provide the stationary balance of the electrons in the N-n-N region. This approach is usually called the "ideal emitter approach", which is widely used in the theory of vertical electron transport in heterostructures. The effect of emitter nonideality on vertical electron transport in different heterostructures was considered previously (see Ref. 17 and the references therein).

At moderate THz irradiation, the effective temperature T is close to the electron temperature in the dark T_{dark}. The latter can be somewhat different from the lattice temperature T_0. However, in the case of the barrier layers with close x and y, one can disregard the difference between T_{dark} and T_0. In this case, Eq. (1) for the THz photocurrent density $\Delta j = j - j_{dark}$ (where $j_{dark} = j\big|_{T=T_0} \propto p_c^{-1}$ is the dark current density) yields

$$\Delta j = j_{dark}\left(\frac{\Delta_C - \mu}{k_B T}\right)\frac{\left(T - T_0\right)}{T_0}\,. \tag{2}$$

The variation of the effective temperature $T - T_0$ associated with the THz irradiation is governed by the energy balance in the G-layer:

$$\frac{k_B\left(T - T_0\right)}{\tau_0^{\varepsilon}} \simeq \frac{D\beta\hbar\Omega I_\Omega}{\Sigma\left(1 + \Omega^2\tau^2\right)}. \tag{3}$$

Here,

$$\tau_0^{\varepsilon} = \tau_0\left(1 + \xi_0\right)\left(\frac{k_B T_0}{\hbar\omega_0}\right)^2 \exp\left(\frac{\hbar\omega_0}{k_B T_0}\right) \tag{4}$$

is the electron energy relaxation time when the electron system in the G-layer is not so far from equilibrium,[3] τ_0 is the characteristic time of the spontaneous emission of optical phonons in the G-layer, D is the Drude weight, $\beta = \pi e^2/\hbar c \simeq 0.023$ (c is the speed of light in vacuum), and Ω and I_Ω are the frequency of the incident THz radiation and its flux, respectively. Moreover, $\xi_0 = \tau_0^{decay} / \tau_0$, where τ_0^{decay} is the optical phonon decay time, and $\hbar$ is the reduced Planck constant. The Drude weight D is equal to $D \simeq (k_B T_0\tau/\pi\hbar)$ if this time is inversely proportional to the electron momentum. This occurs when the dominant electron scattering in the G-layer is associated with acoustic phonons, point defects, and strongly screened Coulomb centers (see, for example, Ref. 18). In the case of several scattering mechanisms, one can assume that the momentum relaxation time is independent of the electron momentum.[19] This assumption leads to the following formula for D:

$$D = \frac{4k_B T_0 \tau}{\pi\hbar} \ln\left[1 + \exp\left(\frac{\mu}{k_B T_0}\right)\right]. \tag{5}$$

In Eq. (3), we have neglected the contribution of the interband absorption in the G-layers in comparison with the intraband (Drude) absorption. This is justified when $D >> 1$ and at a not too high radiation frequency $\Omega < D/\tau$ that is valid for not too high quality G-layers at frequencies up to several THz.

Equations (2) and (3) lead to the following expression for the THz photocurrent density:

$$\Delta j = j_{dark}\left(\frac{\Delta_C - \mu}{k_B T_0}\right)\frac{\tau_0^{\varepsilon} D\beta I_\Omega}{\Sigma\left(1+\Omega^2\tau^2\right)}\left(\frac{\hbar\Omega}{k_B T_0}\right). \tag{6}$$

4. Detector Responsivity and Dark Current Limited Detectivity

The detector responsivity and dark current limited detectivity are typically defined as

$$R_\Omega = \frac{\Delta j}{\hbar\Omega I_\Omega},\ D_\Omega^* = \frac{R_\Omega}{\sqrt{4egj_{dark}}}, \tag{7}$$

respectively, where g is the photoconductive gain, which is equal to $g \simeq 1/p_c$ for detectors with a single absorbing layer under consideration.[14]

Considering these definitions and using the above equations, we arrive at

$$R_\Omega \simeq \frac{R_0}{p_c}\ln\left[1+\exp\left(\frac{\mu}{k_B T_0}\right)\right]\left(\frac{\Delta_C-\mu}{k_B T_0}\right)\exp\left[-\left(\frac{\Delta_C-\mu}{k_B T_0}\right)\right]\frac{1}{\left(1+\Omega^2\tau^2\right)}, \tag{8}$$

and

$$D_\Omega^* \simeq \frac{D_0^*}{\sqrt{\Theta}}\ln\left[1+\exp\left(\frac{\mu}{k_B T_0}\right)\right]\left(\frac{\Delta_C-\mu}{k_B T_0}\right)\exp\left[-\frac{1}{2}\left(\frac{\Delta_C-\mu}{k_B T_0}\right)\right]\frac{1}{\left(1+\Omega^2\tau^2\right)}, \tag{9}$$

where

$$R_0 = \frac{4e\beta}{\pi}\frac{\tau_0^{\varepsilon}}{\hbar},\ D_0^* = \frac{2\sqrt{6}}{\pi^{3/2}}\frac{\beta\tau_0^{\varepsilon}\sqrt{\tau}\upsilon_W}{k_B T_0}, \tag{10}$$

and

$$\Theta = \frac{12}{\pi^2}\int_0^\infty \frac{xdx}{\exp\left(x-\mu/k_BT_0\right)+1}.$$

Here, $v_W \simeq 10^8$ cm/s is the characteristic carrier velocity in G-layers. The factor $1/p_c >> 1$ in Eq. (8) describes an increase in detector responsivity due to photoconductive gain. For realistic heterostructures with G-layers sandwiched between the wide-gap layers of the material under consideration, as well as of such materials as MoS_2, p_c can be fairly small.[16]

As an illustration, Fig. 2 shows the normalized responsivity $R_\Omega p_c/R_0$ and detectivity D^*_Ω / D^*_0 calculated using Eqs. (8)–(10) as functions of the electron Fermi energy μ in the G-layer for different collector barrier heights Δ_C values for the radiation frequencies $\Omega/2\pi$ = 1.0 THz and $\Omega/2\pi$ = 1.5 THz. It is assumed that T_0 = 300 K and τ = 1 ps.

5. Discussion

The characteristic quantities R_0 and D^*_0 are determined by the parameters of the G-layer, so that they are independent of the barrier material. Assuming the optimized Δ_C (Δ_C is a fraction of the energy gap, the latter varies from ~300 meV for the b-P layer to ~150 meV for the b-As layer), one can put $\Delta_C \simeq$ 50−200 meV. In accordance with Eqs. (8) and (9), the maxima of R_Ω and D^*_Ω at T_0 = 300 K are achieved at $\Delta_C - \mu \simeq k_BT_0$ ~25 meV and $\Delta_C - \mu \simeq 2k_BT_0$ ~50 meV, respectively. These conditions can be achieved by selecting x and y for realistic μ values, i.e., the realistic doping of the G-layer. Considering the values of $R_\Omega p_c/R_0$ and D^*_Ω / D^*_0

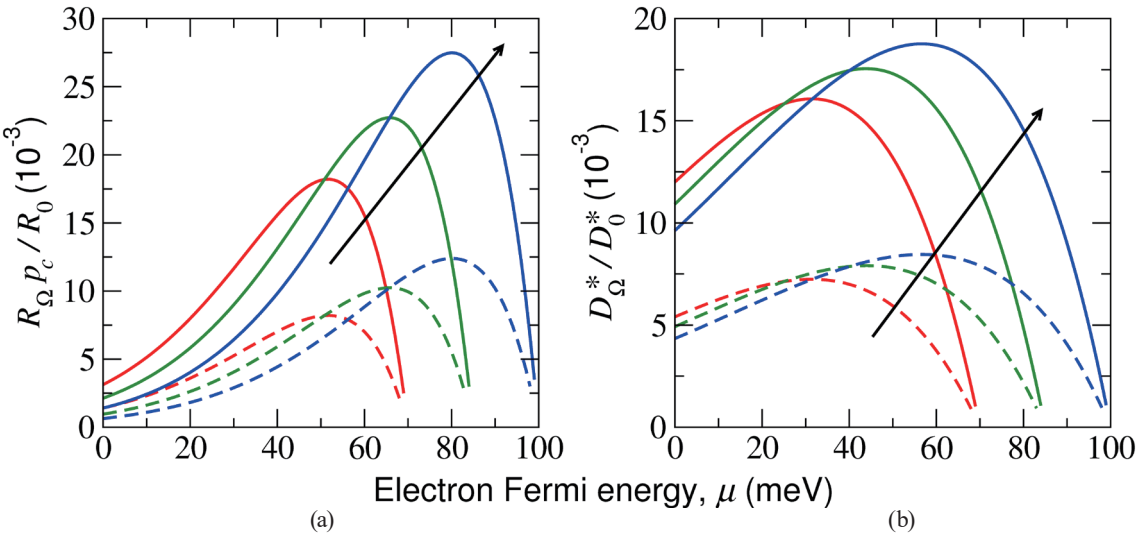

Fig. 2. (Color online) The normalized responsivity $R_\Omega p_c/R_0$ (a) and detectivity D^*_Ω/D^*_0 (b) versus the electron Fermi energy μ in the G-layer for the collector barrier height Δ_C varying from 70 to 100 meV (as indicated by arrows) with a 15 meV increment at $\Omega/2\pi$ = 1.0 THz (solid lines) and $\Omega/2\pi$ = 1.5 THz (dashed lines) (T_0 = 300 K and τ = 1 ps).

corresponding to $\Omega/2\pi$ THz shown in Fig. 2, for the responsivity and detectivity maxima, we obtain $R_\Omega \simeq 40 / p_c$ A/W and $D^*_\Omega \simeq 3\times10^8$ cm$\sqrt{\text{Hz}}$ / W, respectively.

The specific features of the detectors made of the proposed heterostructures and the flexibility of their parameter variation might provide their considerable advantages over G-layer-based detectors with other barrier materials.

Selecting heterostructures with $x > y$, one can obtain rather low capture probabilities because of the high energies of the injected electrons crossing the G-layer. However, a larger emitter barrier height Δ_E in comparison with the collector barrier height Δ_C can lead, as mentioned above, to an undesirable electron heating in the G-layer even under the dark current condition ($T_{dark} > T_0$). This implies that the optimum might be achieved when $x \geq y$.

The coefficient of the THz radiation absorption in the G-layer is relatively small at $\beta \simeq 0.023$. However, the quantum efficiency of the detector under consideration can be markedly enhanced by its integration with a microcavity.[20]

The detectors under consideration use the intraband (Drude) absorption of the THz radiation. The Drude absorption strongly weakens with increasing radiation frequency Ω. This results in a low electron heating efficiency in the frequency range of several THz and above. Therefore, the responsivity and detectivity of the bolometric detectors using such a heating mechanism [see Eqs. (7) and (8)] might be insufficient. However, when $\hbar\Omega \sim \Delta_C / 2$, the interband absorption in the G-layers can result in an effective electron photoemission from these layers. The detectors using this mechanism can exhibit a fairly high performance.[21,22] However, the efficiency of such detectors is limited by the range of sufficiently high photon energies (for example, the detectors based on hBN/G/hBN heterostructures) except for relatively small Δ_C values. In this regard, the b-$As_{1-x}P_x$/G/b-$As_{1-y}P_y$ heterostructure appears to be suitable not only for the detectors using the bolometric effect (at moderate THz frequencies), but also for those using the electron interband photoexcitation (in the range $\hbar\Omega$ ~100 meV, i.e., $\Omega/2\pi$ ~25 THz).

The proposed detectors can surpass the THz detectors based on III-V compounds.[23,24] The latter can operate in the regime of the quantum-well (QW) ionization due to the radiative interband intersubband transitions and in the bolometric regime. In the case of the intersubband QW detectors, the photodetector operation requires the inclined radiation incidence (for the n-type) detectors with the absorption coefficient $\beta^{QW} < \beta$. Apart from this, the capture probability into the QWs is usually higher than that into the G-layers.[15,16] All these factors work in favor of the proposed THz detector. We also compare the bolometric QW-based detectors and the bolometric detectors using the b-$As_{1-x}P_x$/G/b-$As_{1-y}P_y$ heterostructures. Again, such a comparison shows that, owing to a relatively long energy relaxation time in the G-layer, the detectors utilizing the electron heating in the G-layer by the absorbed THz radiation might exhibit a better performance. Indeed, the responsivity and detectivity of the bolometric detectors are proportional to the electron energy relaxation time τ_0^ε in the G-layer [see Eqs. (7)–(10)], which at room temperature is more than an order of magnitude larger than the pertinent energy relaxation times in GaAs, InAs, and InSb QWs (see, for example, Ref. 4).

The properties of the b-$As_{1-x}P_x$/G/b-$As_{1-y}P_y$ heterostructure with layers of n-type and analogous heterostructures with p-layers are fairly similar (the heights of the barriers and the dynamic characteristics of the electrons and holes are not so different). This opens the possibility to create THz detectors using both n- and p-type doped layers.

6. Conclusion

We proposed vertical hot-electron THz detectors based on b-$As_{1-x}P_x$/G/b-$As_{1-y}P_y$ heterostructures using the effects of the electron heating in the G-layer accompanied by the effect of the photoconductive gain. Using the developed device model, we evaluated the detector responsivity and dark current limited detectivity. It was demonstrated that using such narrow-gap barrier materials as b-P and b-As enables a pronounced enhancement of the bolometric THz detector performance.

Acknowledgments

The work at UoA, RIEC, and UB was supported by Japan Society for Promotion of Science (Grants Nos. 16H−06361 and 16K14243). The work at RPI was supported by Office of Naval Research, USA (Project Monitor Dr. Paul Maki).

References

1 A. H. Castro Neto, F. Guinea, N. M. R. Peres, K. S. Novoselov, and A. K. Geim: Rev. Mod. Phys. **81** (2009) 109. https://doi.org/10.1103/RevModPhys.81.109
2 F. T. Vasko and V. Ryzhii: Phys. Rev. B **77** (2008) 195433. https://doi.org/10.1103/PhysRevB.77.195433
3 V. Ryzhii, T. Otsuji, M. Ryzhii, N. Ryabova, S. O. Yurchenko, V. Mitin, and M. S. Shur: J. Phys. D **46** (2013) 065102. https://doi.org/10.1088/0022-3727/46/6/065102
4 V. Ryzhii, A. Satou, T. Otsuji, M. Ryzhii, V. Mitin, and M. S. Shur: J. Appl. Phys. **116** (2014) 114504. https://doi.org/10.1063/1.4895738
5 G. Gong, H. Zhang, W. Wang, L. Colombo, R. M. Wallace, and K. Cho: Appl. Phys. Lett. **103** (2013) 053513. https://doi.org/10.1063/1.4817409
6 Y. Cai, G. Zhang, and Y.-W. Zhang: Sci. Rep. **4** (2014) 6677. https://doi.org/10.1038/srep06677
7 H. Asahina and A. Morita: J. Phys. C: Solid State Phys. **17** (1984) 1839. https://doi.org/10.1088/0022-3719/17/11/006
8 Xi Ling, H. Wang, S. Huang, F. Xia, and M. S. Dresselhaus: PNAS **112** (2015) 4523. https://doi.org/10.1073/pnas.1416581112
9 B. Liu, M. Kopf, A. N. Abbas, X. Wang, Q. Guo, Y. Jia, F. Xia, R. Weihrich, F. Bachhuber, F. Pielnhofer, H. Wang, R. Dhall, S. B. Cronin, M. Ge, X. Fang, T. Nilges, and C. Zhou: Adv. Mater. **27** (2015) 4423. https://doi.org/10.1002/adma.201501758
10 M. Long, A. Gao, P. Wang, H. Xia, C. Ott, C. Pan, Y. Fu, E. Liu, X. Chen, W. Lu, T. Nilges, J. Xu, X. Wang, W. Hu, and F. Miao: Sci. Adv. **3** (2017) e1700589. https://doi.org/10.1126/sciadv.1700589
11 S. Yuan, C. Shen, B. Deng, X. Chen, Q. Guo, Y. Ma, A. Abbas, B. Liu, R. Haiges, C. Ott, T. Nilges, K. Watanabe, T. Taniguchi, O. Sinai, D. Naveh, C. Zhou, and F. Xia: Nano Lett. **18** (2018) 3172. https://doi.org/10.1021/acs.nanolett.8b00835
12 Li Yu, Z. Zhu, A. Gao, J. Wang, F. Miao, Yi Shi, and X. Wang: Nanotech. **29** (2018) 484001. https://doi.org/10.1088/1361-6528/aae05f
13 Y. Chen, C. Chen, R. Kealhofer, H. Liu, Z. Yuan, L. Jiang, J. Suh, J. Park, C. Ko, H. S. Choe, J. Avila, M. Zhon, Z. Wei, J. Li, S. Li, H. Gao, Y. Liu, J. Analytis, Q. Xia, M. C. Asensio, and J. Wu: Adv. Mat. **30** (2018) e1800754. https://doi.org/10.1002/adma.201800754

14 H. C. Liu: Appl. Phys. Lett. **60** (1992) 1507. https://doi.org/10.1063/1.107286
15 E. Rosencher, B. Vinter, F. Luc, L. Thibaudeu, P. Bois, and J. Nagle: IEEE Trans. Quantum Electron. **30** (1994) 975. https://doi.org/10.1109/3.362722
16 V. Ya. Aleshkin, A. A. Dubinov, M. Ryzhii, V. Ryzhii, and T. Otsuji: J. Phys. Soc. Jpn. **84** (2015) 094703. https://doi.org/10.7566/JPSJ.84.094703
17 V. Ryzhii, T. Otsuji, M. Ryzhii, V. Ya. Aleshkin, A. A. Dubinov, V. Mitin, and M. S. Shur: J. Appl. Phys. **17** (2015) 154504. https://doi.org/10.1063/1.4918313
18 V. Ryzhii, D. S. Ponomarev, M. Ryzhii, V. Mitin, M. S. Shur, and T. Otsuji: Opt. Mat. Exp. **9** (2019) 585. https://doi.org/10.1364/OME.9.000585
19 J. N. Heyman, J. D. Stein, Z. S. Kaminski, A. R. Banman, A. M. Massari, and J. T. Robinson: J. Appl. Phys. **117** (2015) 015101. https://doi.org/10.1063/1.4905192
20 M. Furchi, A. Urich, A. Pospischil, G. Lilley, K. Unterrainer, H. Detz, P. Klang, A. M. Andrews, W. Schrenk, G. Strasser, and T. Mueller: Nano Lett. **12** (2012) 2773. https://doi.org/10.1021/nl204512x
21 V. Ryzhii, M. Ryzhii, D. Svintsov, V. Leiman, V. Mitin, M. S. Shur, and T. Otsuji: Infrared Phys. Technol. **84** (2017) 72. https://doi.org/10.1016/j.infrared.2017.01.016
22 V. Ryzhii, M. Ryzhii, V. Leiman, V. Mitin, M. S. Shur, and T. Otsuji: J. Appl. Phys. **122** (2017) 054505. https://doi.org/10.1063/1.4997459
23 M. Graf, G. Scalari, D. Hofstetter, J. Faist, H. Beere, E. Linfeld, D. Ritchie, and G. Davies: Appl. Phys. Lett. **84** (2004) 475. https://doi.org/10.1063/1.1641165
24 H. C. Liu, C. Y. Song, A. J. SpringThorpe, and J. C. Cao: Appl. Phys. Lett. **84** (2004) 4068. https://doi.org/10.1063/1.1751620